In preparation for a journal

New and Better Near-Infrared Detectors for the *JWST* Near Infrared Spectrograph

Bernard J. Rauscher, D. Brent Mott, Yiting Wen, Don Lindler[2],
Matthew A. Greenhouse, and Robert J. Hill[1]

NASA Goddard Space Flight Center, Greenbelt, MD, 20771, USA

Bernard.J.Rauscher@nasa.gov

ABSTRACT

ESA and NASA recently selected two 5 μm cutoff Teledyne H2RG sensor chip assemblies (SCA) for flight on the James Webb Space Telescope (*JWST*) Near Infrared Spectrograph (NIRSpec). These HgCdTe SCAs incorporate Teledyne's "improved barrier layer" design that eliminates the degradation that affected earlier *JWST* H2RGs (Rauscher et al. 2012a). The better indium barrier, together with other design changes, has improved the performance and reliability of *JWST*'s SCAs. In this article, we describe the measured performance characteristics that most directly affect scientific observations including read noise, total noise, dark current, quantum efficiency (QE), and image persistence. As part of measuring QE, we measured the quantum yield as a function of photon energy, Φ, and found that it exceeds unity for photon energies $E_\gamma > (2.65 \pm .2)\ E_g$, where E_g is the HgCdTe bandgap energy. This corresponds to $\lambda \lesssim 2$ μm for NIRSpec's 5 μm cutoff HgCdTe. Our measurements agree well with a previous measurement by McCullough et al. (2008) for $\Phi \lesssim 1.3$. For $\Phi > 1.3$, we find a slower increase in Φ with photon energy than McCullough et al. did. However, and as McCullough et al. note, their "two state" model of the yield process is not valid for large $\Phi \gg 1$.

Subject headings: instrumentation: detectors

1. Introduction

ESA and NASA recently selected two 5 μm cutoff HgCdTe Teledyne H2RG SCAs for flight on the *JWST* NIRSpec. These are the two "best" H2RGs out of eight candidates that were

[1]Conceptual Analytics, LLC, Glenn Dale, MD, USA

[2]Sigma Space Corporation, 4600 Forbes Blvd., Lanham, MD, 20706, USA

available. The new H2RGs incorporate Teledyne's "improved barrier layer" design to eliminate the degradation that affected older *JWST* H2RGs (Rauscher et al. 2012a). They also incorporate a few other design changes that have reduced the read noise and crosstalk compared to previous *JWST* H2RGs.

To qualify the new design, NASA and Teledyne conducted extensive destructive physical analysis, environmental testing, and accelerated life testing (Rauscher et al. 2012a, 2013b). Our focus here is on the performance testing. Sec. 2, and especially Tab. 1, present the flight selection performance results. These show that the new flight parts generally meet NIRSpec requirements[1] with margin. We believe that this performance represents today's state-of-the-art for 5 μm cutoff H2RGs. Sec. 2 discusses the summary table and performance measurements in more detail.

To provide some insight into the pool of available NIRSpec SCAs, we provide detailed information for the six "flight candidates" that were not selected as well as the two SCAs that were. Of the eight NIRSpec SCAs that passed Teledyne's screen testing (the "flight candidates"), two were deemed flight grade, another two were almost as good and are currently "flight spares", three had minor issues of one kind or another, and one had anomalously bad persistence. The Teledyne screen testing was designed to eliminate parts with severe problems such as large photo-emissive defects. Detailed performance characterization testing was done in the Goddard Detector Characterization Laboratory (DCL). In addition to the eight "flight candidate" SCAs that we report on here, there were a few others that failed screen testing. Of the parts that passed screen testing, at least one quarter are considered flight grade.

When energetic short wavelength photons interact with the HgCdTe, they can create more than one electron-hole pair per incident photon. As part of measuring the QE, we measured this quantum yield, Φ as a function of photon energy. Sec. 3 describes the physical process and the new measurements which are in good agreement with a previous measurement by McCullough et al. (2008) for $\Phi \lesssim 1.3$. In Sec. 3 we show that the onset threshold for quantum yield is about $2.65 \pm .2$ E_g, where E_g is the bandgap energy. When the quantum yield becomes larger than $\Phi \gg 1.3$, we find that Φ increases more slowly with photon energy than McCullough et al. did. However, in Sec. 8 of McCullough et al., the authors point out that their "two state" model becomes invalid when the quantum yield is large. To within the uncertainties, therefore, we believe that our results are in good agreement with McCullough et al. except where the yield is so large that McCullough et al.'s model does not apply.

Now that the performance of the new H2RGs is known, the flight SCAs are being built into a new focal plane assembly (FPA) at NASA Goddard Space Flight Center and Exelis in Rochester, NY. The FPA will in turn be integrated with a pair of SIDECAR ASICs for H2RG control, focal

[1]The *JWST* NIRSpec "requirements" are formally defined in a series of *JWST* project documents. Although these documents capture exactly what is needed, they are often not comprehensible without reading other *JWST* documents. In the interest of brevity, we therefore use the work "requirement" informally in this manuscript. The relevant *JWST* project document always takes precedence.

plane electronics (FPE) for SIDECAR and thermal control, and assorted harnesses and software to form a new "NIRSpec detector subsystem". We will characterize the complete detector subsystem prior to integrating it into the NIRSpec instrument.

Our aims in this article were two fold. Firstly, we wanted to present the measured performance of the two NIRSpec flight SCAs for the benefit of potential *JWST* observers. We believe that the measured performance is consistent with today's state-of-the-art for 5 μm cutoff H2RGs. In doing this we have tried to present enough information on the six parts that were not selected as well as the best two in order to provide insight into how our flight build went. We are hopeful that this information may prove helpful to others who are planning large SCA procurements. Finally, we anticipate that some of the measured characteristics may prove useful to other instrument builders.

A second aim was to present the quantum yield measurements for the *JWST* 5 μm SCAs. Reassuringly, our results are consistent with previous work by McCullough et al. (2008) to within 2% for all wavelengths $\lambda \geq 900$ nm. For $\lambda < 900$ nm, we believe that our empirical approach is likely to be more reliable than the quantum yield inferred using McCullough et al.'s model which is most applicable to quantum yields near unity.

2. Performance characteristics

The performance testing was done in the Goddard Detector Characterization Laboratory's (DCL) "Purple Dewar" using a Gen-III Leach controller. This is the same test setup that we have previously used for NIRSpec testing (Moseley et al. 2010; Mott et al. 2008, 2007; Rauscher et al. 2013a, 2012b,a, 2011b,a, 2008, 2007a). The Purple Dewar has a demonstrated dark current floor of < 0.003 e^- s^{-1} for 5 μm cutoff detectors and read noise per CDS floor of < 7 e^- rms. The Purple Dewar can accommodate two SCAs at a time. The SCAs are operated at T $\approx$ 38.5 K. Temperature was actively controlled to δT < 1 mK over the approximately two week test duration using a Lakeshore temperature controller. Appendix B provides more detail on the specific test configuration including the bias voltages and gain settings that we used. The Purple Dewar is described in more detail in Mott et al. (2008, 2007). We recently upgraded the Purple Dewar's absolute QE calibration as described in Appendix A.

For most observations, NIRSpec uses a standard "baseline science integration" (BSI). In a BSI, the detector is reset using the the H2RG's enhanced clocking mode with the pixel-by-pixel reset at the nominal frame rate. Following one reset frame, we collect 88 non-destructively sampled up-the-ramp frames at a 10.5472 seconds per frame cadence.[2] The resulting integration for the ground testing that is described in this paper is time is 917.608 seconds. For more information on the NIRSpec readout mode, we refer the interested reader to Rauscher et al. (2007b).

[2]When the SIDECAR ASIC is used for SCA control, the frame time goes up slightly, but in any case the frame time will be shown in the FITS header.

Tab. 1 summarizes the measured performance versus requirements. The two flight SCAs are SCA17163 and SCA17280. These SCAs comprehensively meet NIRSpec requirements apart from a narrow range of wavelength near the AR coating's minimum transmission where there is a small deviation. In the following paragraphs we describe some of the parameters in more detail. At the end of this section we explain why these two SCAs were selected for flight.

Table 1: DCL performance measurements

			NIRSpec flight candidate SCA serial number[1]							
Parameter	Req.	Unit	**17163**	**17280**	17167	17169	17378	17168	17166	17195
Flight application:										
NIRSpec flight SCA identifier			**491**	**492**	N/A	N/A	N/A	N/A	N/A	N/A
Flight ranking			**1**	**2**	3	4	5	6	7	8
NIRSpec requirements:										
Mean dark current per pixel	< 0.01	e^-/s/pix	**0.0032**	**0.0041**	0.0051	0.0027	0.0043	0.0032	0.0043	0.0047
Latent or residual images	< 0.1%	%	**0.009**	**0.013**	0.019	0.012	0.014	0.016	0.009	0.063
Total noise per pixel[2]	< 6	e^- rms	**< 4.32**	**< 5.18**	< 4.8	< 5.19	< 5.07	< 5.02	< 4.46	< 5.8
Mean DQE										
$0.6 < \lambda < 1$ μm	≥ 70%	%	**79.5**	**80.4**	78.9	83.9	86.5	75.8	89.4	81.5
$1 \leq \lambda < 5$ μm	≥ 80%	%	**88.0**	**88.3**	87.2	85.9	91.0	80.6	88.7	88.1
Pixel operability for science observations	> 89%	%	**99.02**	**98.25**	98.92	98.06	97.7	98.65	98.91	97.74
Pixel cross talk	< 5%	%	**0.54**	**0.49**	0.52	0.62	0.6	0.61	0.52	0.48
Other information:										
Test start date		MM/YY	**08/13**	**09/13**	08/13	09/13	11/13	10/13	10/13	11/13
Conversion gain		e^-/DN	**0.873**	**0.978**	0.935	0.94	0.904	0.925	0.882	0.946
Transimpedance gain		$\mu V/e^-$	**4.372**	**3.903**	4.082	4.060	4.222	4.126	4.327	4.035
Read noise per CDS[2]		e^- rms	**< 7.4**	**< 8.9**	< 7.9	< 9.1	< 8.4	< 8.3	< 7.4	< 8.8
Open pixels		# pix	**470**	**63**	7	0	0	863	1292	357
RTN pixels		%	**3.3**	**4.0**	2.3	4.3	3.6	3.2	2.7	3.6
Snowball rate		snowballs/hr	**0.66**	**0.02**	0.17	0.14	0.20	0.07	0.07	0.03
Bad rows		#	**0**	**0**	0	0	0	1	0	0
Void pixels		%	**< 1**	**0**	1	< 1	3	3	10	0
Cutoff wavelength from PEC		μm	**5.45**	**5.37**	5.42	5.44	5.47	5.32	5.41	5.36

[1] The two flight SCAs are displayed in boldface font.

[2] These values are an upper limit and the apparent differences are not necessarily real. The test controller was injecting variable $1/f$ noise during the test. This was fixed by moving a card.

2.1. Discussion of individual parameters

2.1.1. Total noise

NIRSpec defines total noise as the standard deviation, computed per pixel, in a stack of > 40 dark BSIs. The NIRSpec requirement is $\sigma_{\rm total} < 6\ e^-$ rms after reference correction. For these tests we used a traditional (for astronomy) reference correction scheme. The detector is read out single-ended and the reference output is not used. Each 2048×2048 pixel "frame" of H2RG data contains a 2040×2040 pixel array of regular pixels that is surrounded on all sides by a 4-pixel wide border of reference pixels. The integrated signal in each pixel is computed using 2-parameter least squares fitting. After fitting slopes, we compute the mean value of reference pixels on the "top" and "bottom" of each output and fit a slope between them. We subtract this to remove output-to-output bias jumps. We then subtract a smoothed column of all reference pixels in columns from each column of the image.

In practice, there are many ad-hoc ways of using the reference pixels in rows and columns like this, and each group tends to do it differently. We have found that the simple approach that we describe above is close to optimal when one does not have access to: (1) the reference output and (2) one has not measured the statistical correlations between the reference pixels and regular pixels. With the laboratory controller that is used here, the difference between this approach and statistically optimal methods is small. With the flight system that uses Teledyne's SIDECAR ASIC, we plan to use statistically optimal methods. We refer the interested reader to our papers on Improved Reference Sampling and Subtraction (IRS^2; pronounced "IRS square") for more information on how to optimally use all of the reference information to reject correlated noise.

2.1.2. Pixel operability

Pixel operability for science is a NIRSpec-specific parameter. Pixels are flagged as "inoperable" if the total noise is $> 12\ e^-$ rms or the QE deviates by more than 30% from the mean value. Defined in this way, many of the "inoperable" pixels still generate useful information. We anticipate that observers will keep as many pixels as possible, even if some of them are formally considered to be "inoperable".

2.1.3. Pixel crosstalk

For NIRSpec, pixel crosstalk is the fraction of the signal that appears in each of the four nearest neighbors. For flight selection, we computed crosstalk by examining hot pixel neighbors and well centered cosmic ray hits. Although the cosmic ray hits include charge diffusion whereas hot pixel neighbors do not, in practice we find that the two methods give the same result to within the uncertainties for these SCAs. Computed in this way, crosstalk is identical to the inter-pixel

capacitance alpha term that Moore et al. (2004) first introduced.

2.1.4. Open pixels

An "open pixel" is a pixel that behaves as if it were missing the indium interconnect between the HgCdTe detector layer and the readout integrated circuit (ROIC). Open pixel are particularly troublesome because there is no potential minimum at their pixel location to collect charge. The charge therefore collects in neighboring pixels creating a bright "donut" around the affected pixel. Because of this "donut", each open pixel corrupts about five pixels including itself.

2.1.5. RTN pixels

Random telegraph noise (RTN) can appear as an almost digital toggling on and off between states in up-the-ramp sampled data (*i.e.* as if the pixel were sending a message in morse code). RTN is thought to be caused by single charges moving on to and off of isolated quantum defect states in individual pixel MOSFETs. Although RTN can manifest in a great many ways (Bacon et al. 2005), from an observer's perspective it is best thought of as non-Gaussian noise that affects individual pixels. Because of their non-Gaussian noise, RTN pixels will require special handling in the calibration pipeline.

2.1.6. Snowball rate

Snowballs may well be unique to space missions and others who are in the fortunate position of receiving detectors very soon after they are made. Snowballs appear to be much like an enormous cosmic ray hit, often affecting ~ 100 pixels. In *JWST*, we have found that the snowball rate goes down with time, and moreover the decay rate is consistent with known radioactive isotopes that are used during the SCA fabrication process at Teledyne. Snowballs are the reason why this table also contains the test start date. By the time *JWST* flies in 2018, we believe that the snowball rate will be negligible.

2.1.7. Void pixels

JWST's H2RGs are manufactured using flip-chip hybridization. The ROIC and HgCdTe detector layer are fabricated separately. They are subsequently hybridized using indium bump bonds and an epoxy is wicked between the bumps to increase the mechanical strength.

During the *JWST* flight production, we experienced non-uniform epoxy backfill that created voids (see Fig. 1-2). The voids flatfield out from science data. Extensive thermal cycling by the

JWST project and finite elements modeling by Teledyne show that the voids are mechanically stable with excellent strength margin versus growth. Nevertheless, for NIRSpec we were in the fortunate position of having excellent parts that had very small (or nonexistent) voids. The voids were therefore considered as only one factor among many in ranking the SCAs.

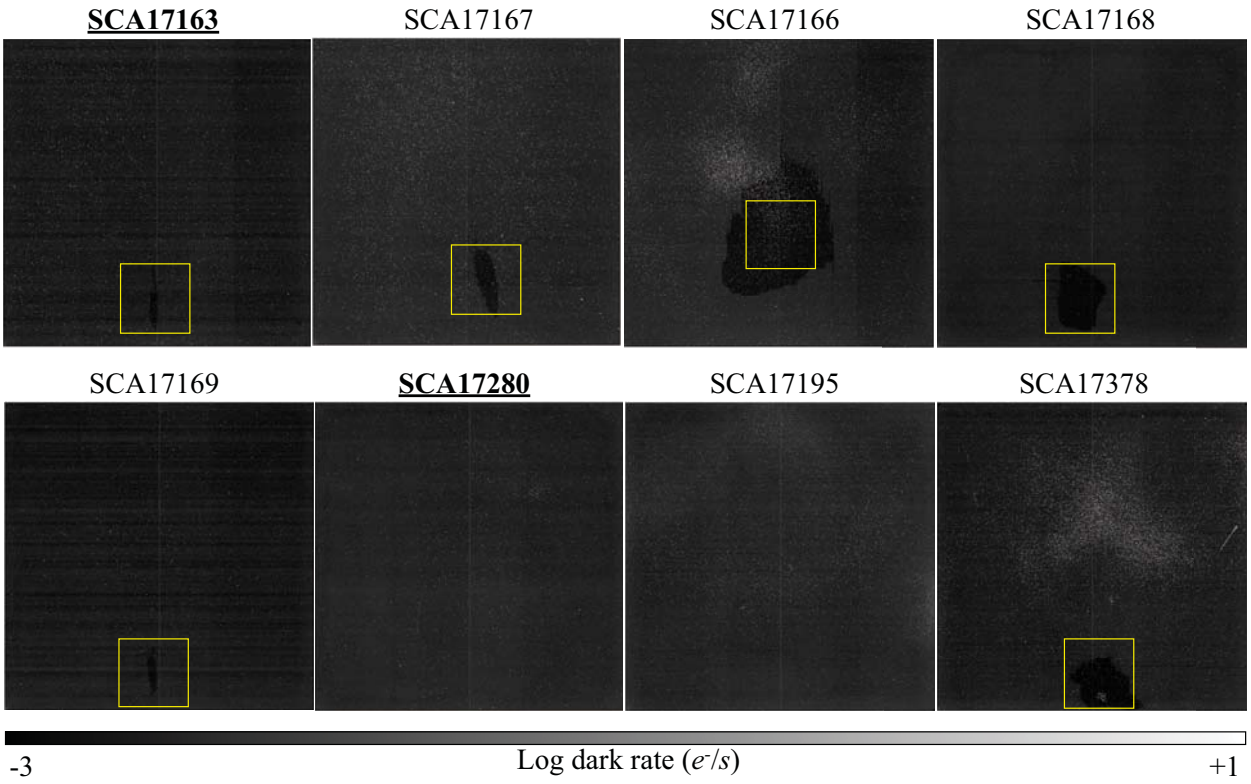

Fig. 1.— This figure displays the dark maps of all eight flight candidates on the same grayscale. The two flight parts are indicated by underlined boldface type. Six of the parts had noticeable epoxy voids. These are indicated by the light box which encapsulates 5% of the pixelated area.

2.1.8. Quantum efficiency

QE is the probability that an incident photon will promote charge carriers into conduction in the semiconductor. One simple way of measuring QE is to expose the detector to a known illumination stimulus and measure the response. The ratio of the response to the stimulus is the responsive quantum efficiency (RQE). For energetic short wavelength photons which can create more than one electron hole pair in the HgCdTe, RQE tends to over estimate QE. However, QE can be inferred from RQE data if the quantum yield, $\Phi(\lambda)$, is known and divided out from the RQE data.

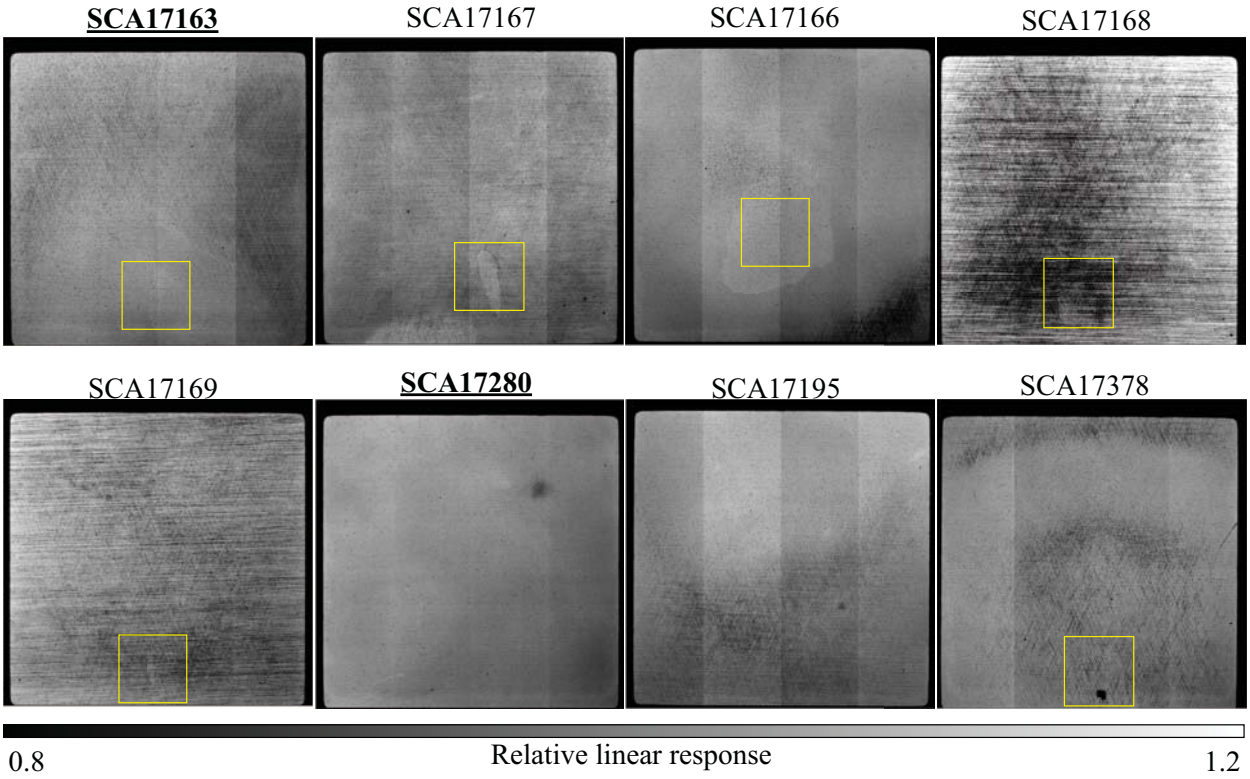

Fig. 2.— This figure shows the 2 μm flatfield images of all eight flight candidates. The two flight parts are indicated by underlined boldface type. Six of the parts had noticeable epoxy voids. These are indicated by the light box which encapsulates 5% of the pixelated area. The edges on three sides are vignetted by a field stop in the test setup. Pixels in the vignetted areas appear dark. The flatfield images show faint "crosshatching" (see also Sec. 2.2) that is caused by dislocation defects in the HgCdTe. These defects, which flatfield out, follow the HgCdTe crystal lattice planes and are inherent in the manufacturing process.

Fig. 3 shows the QE that we inferred from our RQE data for the two flight SCAs. We discuss the quantum yield correction further in Sec. 3. For NIRSpec's 5 μm cutoff HgCdTe, the quantum yield exceeds unity for wavelength $\lambda \lesssim 2$ μm.

2.1.9. Persistence

Persistence refers to the charge memory from an earlier exposure appearing in the current one. It is important because bright sources in one exposure can affect subsequent exposures by imprinting latent ghost images. Although these can be mitigated in calibration pipelines, good practice dictates choosing SCAs that have minimal persistence.

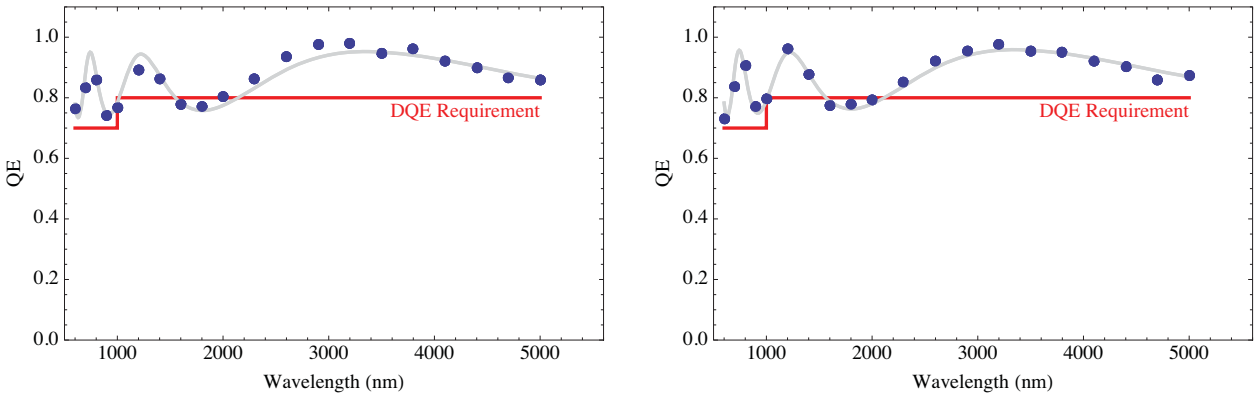

a) SCA17163 b) SCA17280

Fig. 3.— This figure shows $QE(\lambda) = RQE(\lambda)/\Phi(\lambda)$ for the two flight SCAs. There is about a $\pm 6\%$ correlated (*i.e.* systematic) uncertainty on all data points. The statistical error bars are about 2.5%. To provide context, we overlay the NIRSpec QE requirements in red and a two parameter non-linear least squares fit of Teledyne's theoretical AR coating model in gray (Eq. 4 with α and β fixed).

When the *JWST* project started working with Teledyne in the early 2000s, we defined a fairly simple persistence requirement and test procedure. We now know that both the requirement and procedure are inadequate. Most current *JWST*'s H2RGs easily meet the $< 0.1\%$ persistence requirement that we wrote then. However, that simple requirement did not capture all aspects of persistence that are important for scientific observations. Since then, a fairly clear consensus has emerged regarding latent persistence images in *JWST* H2RGs.

Testing by the *JWST* Near Infrared Camera (NIRCam) team shows that persistence has the following properties (Leisenring et al. 2014);

- latents do not depend on wavelength of illumination,
- latents do not get stronger past $\sim 3\times$ saturation,
- latents are weaker for 5 μm cutoff detectors,
- taking longer to apply a given level of illumination causes a stronger latent image than a shorter time, and
- latent strength does not depend on whether the illumination is focused or flat field.

Mike Regan of STScI and Roger Smith of CalTech have studied latents extensively and reached similar conclusions. In addition they find;

- latents depend on position on the detector (*i.e.* there is a latent pattern), and
- there can be a very long wait following detector bias changes while persistent charge decays away.

Both Smith et al. (2008) and Anderson et al. (2014) report that bias settings can be used to mimic persistence in the lab. We have also found this to be true, although we believe that there may be some subtle differences between electronic persistence and persistence from light that would benefit from further study.

Because persistence results can be highly dependent on the details of how the test is executed, we provide more detail on the persistence than for other test procedures. We measured persistence using 10× saturated $\lambda = 3.4$ μm flatfield light. We were careful to use continuous illumination because our own experience, and that of others in the community, has been that long exposures to saturating light cause more persistence than short exposures of the same fluence. Our procedure was as follows.

1. Pre-Dark test:
   (a) Take 2 sequential 918 s up-the-ramp sampled dark integrations
2. 10× Full Well illumination:
   (a) Turn on the cold 3.4 μm LED.
   (b) Adjust the LED current to $\approx 10^4$ e^- s^{-1} pix^{-1}
   (c) Take one 622 s up-the-ramp sampled illuminated integration
   (d) Turn off the cold LED
3. Post-Dark test:
   (a) Take 10 sequential 918 s up-the-ramp sampled dark integrations

Fig. 4 shows the result for the two flight SCAs. We found that the persistence of all eight flight candidates was well approximated the power law, $f(t) = f_0/t$. All of the parts but one produced persistence curves similar to Fig. 4. The one exception was SCA17195 which had anomalously high persistence and a correspondingly larger normalization. The power law index was the same as for the other parts.

The $1/t$ form of the persistence curves is reassuring as it says that most traps decay quickly. It arises naturally from a population of exponentially decaying charge traps, for which the initial trap density of specified decay timescale τ is proportional to $1/\tau$. For present purposes, however, the main point is an empirical one. Persistence in NIRSpec's flight SCAs decays according to a $1/t$ power law and there is no evidence of any long timeconstant persistent tail that would complicate either flight operations or calibration.

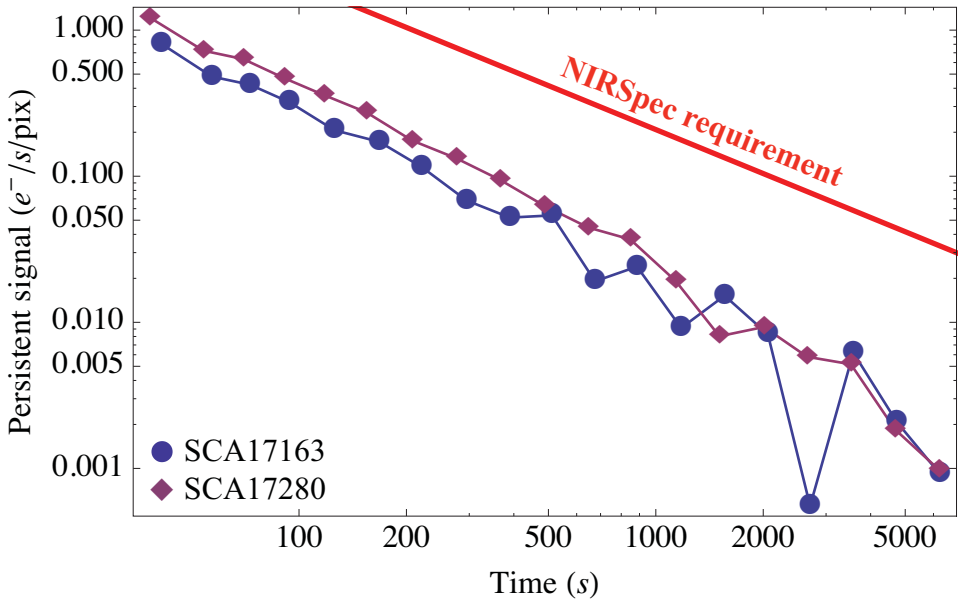

Fig. 4.— The persistence of the two flight parts easily meets the NIRSpec requirement that is shown by the thick red line. For both flight parts, the persistence decay is reasonably well fitted by an $\approx 1/t$ power law. The persistence of five other flight candidates was very similar. Only SCA17195, which had anomalously high persistence, failed to meet the NIRSpec requirement. Even SCA17195 followed the simple power law form, only with a higher normalization.

2.1.10. Performance Summary

Overall, we believe that the "improved barrier layer" design had produced better H2RGs than *JWST* had before. The persistence decays according to a simple power law without any sign of enhanced long timescale persistence. The QE is uniformly higher than in previous *JWST* H2RGs and the shape of the QE curves is consistent with theoretical expectation. Finally, the read noise and dark current are lower. In extensive *JWST* testing at Goddard, the University of Arizona, and Teledyne, we have not noticed any parameter to be worse in the new SCAs, although many parameters seem to be better. This bodes well for *JWST*, *EUCLID*, and *WFIRST*; all of which plan to use Teledyne HxRG family detectors with the new barrier layers.

2.2. Reasons for flight selection

SCA17163 and SCA17280 were selected for flight primarily because they had very low persistence and also because they had comparatively uniform flat field structure. Other considerations included good overall performance and a desire to minimize void size.

We placed particular emphasis on persistence and flat field uniformity because these parameters affect calibration complexity. For example, persistence injects position and time dependent correlations into dithered data sets. For NIRSpec, the most concerning type of flatfield non-uniformity is the "crosshatch" pattern that is visible in Fig. 2. The crosshatching is caused by a fixed pattern of dislocation defects in the HgCdTe. These are inherent in the manufacturing process. The crosshatching flatfields out. However, because crosshatching injects high spatial frequency structure into the flats, it will complicate the NIRSpec calibration pipeline which interpolates flats for any frequency using a library of 20 reference flats. For NIRSpec, we were in the fortunate position of having several good SCAs to choose from. We therefore chose the two that are likely to be easiest to calibrate.

3. Quantum yield

When short wavelength, high energy photons interact with the HgCdTe, they can create more than one electron-hole pair per incident photon. The quantum yield, Φ, increases the RQE,

$$\mathrm{RQE} = \mathrm{QE}\,\Phi, \tag{1}$$

but it also adds Fano noise (Fano 1947). The combined effect of the boosted response and added Fano noise is to reduce the sensitivity compared to a detector that has $\Phi = 1$ and $F = 0$. For both detector characterization and scientific observations, it is therefore important to know when the quantum yield exceeds unity and account for it.

To measure $\Phi(\lambda)$, we asked Teledyne to provide their theoretical AR coating model for our SCAs, $T(\lambda)$. This took the form of a table that gave the predicted transmission as a function of wavelength from $400 - 6000$ nm at 5 nm intervals. Teledyne also provided AR coating witness samples for each SCA, but we found that the theoretical AR coating always gave lower chi-square when fitted to our data. To infer $\Phi(\lambda)$, we fitted $T(\lambda)$ to the RQE data from all eight 5 μm cutoff NIRSpec H2RGs.

Our RQE model was,

$$\mathrm{RQE}\,(\lambda) = \eta T\,(\kappa\lambda)\,\Phi\,(\lambda)\,, \text{ where} \tag{2}$$

$$\Phi(\lambda) = \max\left[1,\ 1 + \beta h c q_e^{-1}\left(\lambda^{-1} - \alpha\lambda_{\mathrm{co}}^{-1}\right)\right]. \tag{3}$$

Eq. 3 is based on the work of Shockley (1961), and in particular it approximates the behavior shown in his Figs. 3-4 to first order in E_γ. In Eqns. 2-3, α is the threshold energy as a fraction of the bandgap energy E_g, β is the slope of the quantum yield after it turns on in units of eV^{-1}, η is the "internal QE", and κ is a wavelength scale factor. κ is needed as a free parameter because Teledyne's anti-reflection coating model is for a different temperature than NIRSpec's T $\sim$ 40 K SCA operating temperature and we expect the AR coating transmission function to shift in wavelength with temperature. Although we refer to η as "internal QE", one should bear in mind that any spectrally

featureless reduction in the QE (e.g. an imperfect AR coating) would be accounted for by η. Substituting Eq. 3 into Eq. 2, we arrive at the 4-parameter expression that we fitted to the data,

$$\mathrm{RQE}\,(\lambda) = \eta T\,(\kappa\lambda)\max\left[1,\ \beta hcq_e^{-1}\left(\lambda^{-1} - \alpha\lambda_{\mathrm{co}}^{-1}\right)\right]. \tag{4}$$

The fits were simple 4-parameter least squares fits. The mean values across all eight SCAs for the fitted parameters are; $\alpha = 2.65 \pm .2$, $\beta = 0.460 \pm .06$ eV^{-1}, $\eta = 0.952 \pm .03$, and $\kappa = 0.930 \pm .02$. Fig. 5 shows the fits for the two flight SCAs and Tab. 2 shows the fit parameters for every SCA. Fig. 6 shows our quantum yield results in the context of McCullough et al.'s work and results for a few other semiconductors from the literature.

Table 2: Results of 4-parameter fitting

SCA	rms of fit	"Internal QE" η	Wavelength scaling κ	Threshold energy α	Slope parameter β (eV^{-1})
SCA17163	0.0226	0.9689	0.9196	2.9048	0.4124
SCA17166	0.0178	0.9587	0.9065	2.5869	0.5489
SCA17167	0.0203	0.9597	0.9438	2.9154	0.4358
SCA17168	0.0101	0.8785	0.9302	2.5832	0.4664
SCA17169	0.0158	0.9346	0.9021	2.6737	0.4969
SCA17195	0.0272	0.9600	0.9388	2.4592	0.4281
SCA17280	0.0279	0.9612	0.9230	2.2680	0.3829
SCA17378	0.0255	0.9940	0.9761	2.8280	0.5110
Mean	0.0209	0.9519	0.9300	2.6524	0.4603
Stddev	0.0062	0.0338	0.0236	0.2263	0.0557

McCullough et al. measured a threshold energy of $E_t = 0.65 \pm .06$ eV using an older 5 μm cutoff NIRSpec H2RG that we provided. This corresponds to $\alpha \sim 2.9 \pm .3$. Here we have used a different but complementary method to measure $\alpha = 2.65 \pm .2$. Moreover, our quantum yield measurements agree with McCullough et al.'s to $< 2\%$ for all $\lambda \geq 900$ nm. For $\lambda < 900$ nm, we do not necessarily expect good agreement. As McCullough et al. emphasize, the conversion relation that they give in their Sec. 8 breaks down when incident photons are likely to generate more than two electron-hole pairs. This is certainly the case in NIRSpec's $\lambda_{\mathrm{co}} \sim 5.4$ μm cutoff HgCdTe for $\lambda < 900$ nm.

Based on the goodness of the fits and reasonable comparisons to other measurements in the literature, we believe that the average quantum yield parameters reported here are reasonable for 5 μm cutoff HgCdTe. We therefore use the measured average values of $\alpha = 2.65 \pm .2$ and $\beta = 0.460 \pm .06$ eV^{-1} in all other sections of this paper.

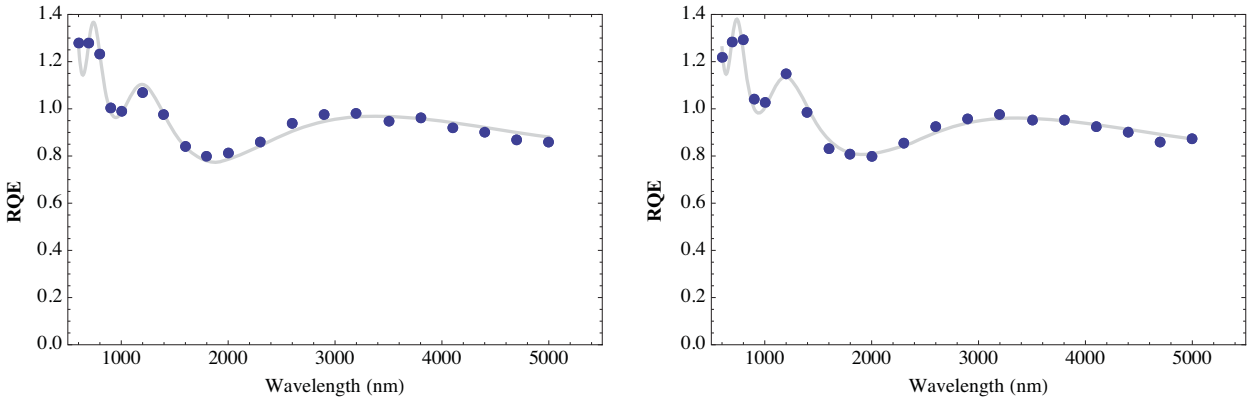

a) SCA17163 b) SCA17280

Fig. 5.— To measure the quantum yield vs. wavelength, $\Phi(\lambda)$, we fitted Eq. 4 to eight NIRSpec flight candidate SCAs. Here we show the fits for the two parts that were selected for flight. The fits for the other six SCAs are similar. The effect of the quantum yield is obvious for wavelengths shorter than 1400 nm, where the RQE usually exceeds 100%. Fig. 3 shows the quantum efficiency, QE, after correcting for quantum yield. As in Fig. 3, there is about a ±6% correlated uncertainty on all data points. The statistical error bars are about 2.5%.

4. Summary

In this article we report the measured performance of the two *JWST* NIRSpec flight SCAs. These SCAs supersede any others that may have previously been designated "flight" parts. The measured performance as shown in Tab. 1 generally meets NIRSpec requirements, and we believe represents today's state of the art for Teledyne's 5 μm cutoff H2RGs. Of the eight SCAs that passed Teledyne's coarse "screen testing", two were deemed "flight" grade, another two were nearly as good, and three others would certainly be desirable in a less demanding application than the *JWST* NIRSpec. Only one of the eight parts that passed the "screen test" clearly had a problem. For this one part, the persistence failed to meet requirements.

As part of characterizing the new detectors, we measured the quantum yield of Teledyne's 5 μm cutoff HgCdTe. Reassuringly, our results were within 2% of McCullough et al. (2008)'s for all wavelengths $\lambda \geq 900$ nm. For $\lambda < 900$ nm, we used an empirical to measure a systematically smaller quantum yield correction than McCullough et al.. Ongoing *JWST* testing at Goddard, STScI, and elsewhere should provide further insight into the correct form of the quantum yield correction at the shortest *JWST* wavelengths.

This work was supported by NASA as part of the James Webb Space Telescope Project. We are very grateful to John Auyeung of Teledyne, who manages the *JWST* work there, and to Eric Piquette, who is our Teledyne HgCdTe lead. Both did a fantastic job making the new detectors

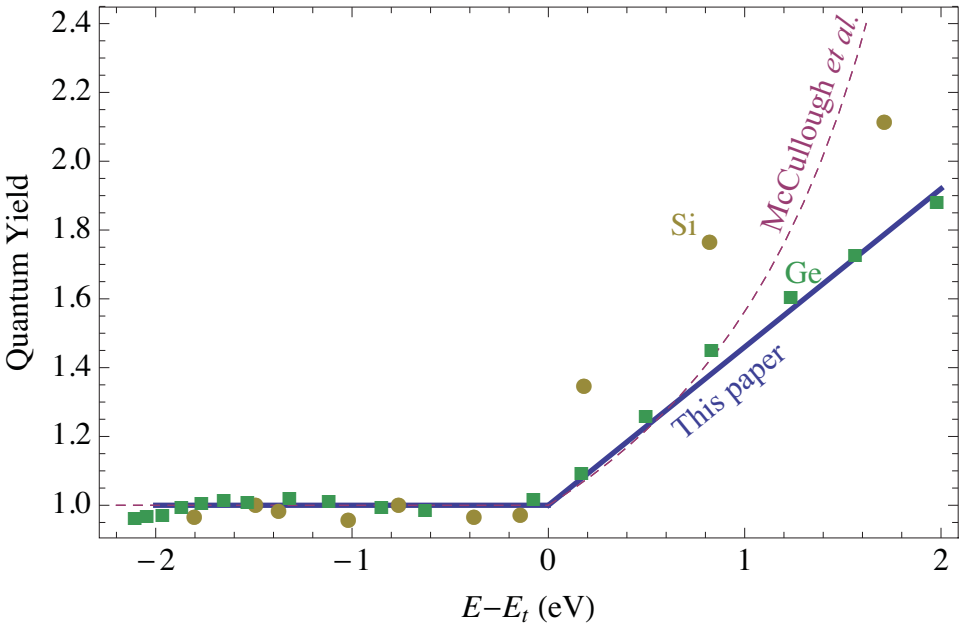

Fig. 6.— This plot shows the fitted quantum yield as a function of wavelength with a few results from the literature to provide context. The data for Si and Ge are from Shockley (1961) and references therein. As is discussed in the text and emphasized by the authors, McCullough et al.'s (2008) model begins to break down for $E - E_t \gtrsim 0.73$ eV ($\lambda < 900$ nm for a NIRSpec SCA). For all wavelengths $\lambda \geq 900$ nm, our model agrees with McCullough et al.'s model to within 2%.

possible.

A. NIST traceable absolute quantum efficiency

Here we describe Goddard Detector Characterization Laboratory's (DCL) the absolute quantum efficiency calibration, which was recently upgraded to be National Institute of Standards and Technology (NIST) traceable.

The Purple Dewar uses two NIST-traceable Judson J10D-FP600765 InSb photodiodes for absolute quantum efficiency calibration. Fig. 7 shows a block diagram of the Purple Dewar when it is configured for quantum efficiency measurements. One InSb diode is mounted in the integrating sphere, where it monitors the intensity of the incoming light. The second is mounted in the focal plan, where it is used to compute the transfer function from the integrating sphere to the focal plane. Once this transfer function is known, only the InSb diode in the integrating sphere is needed to make the measurement.

The DCL's InSb diode calibration is described in detail in a report that NIST delivered to the

DCL. NIST's methodology is described in Podobedov et al. (2012). In practice, the DCL diodes are tertiary standards. The primary standard is NIST's absolute cryogenic radiometer. The NIST team used this to calibrate two "cryogenic working standard" diodes of type J10D-M210S-R07M (NIST Standards #4 and #1). NIST then calibrated the DCL diodes against these using the substitution method that is described in TBD. According to NIST, the 1-σ uncertainty in the DCL reference diode calibration is $\pm 1.5\%$.

The Purple Dewar can be configured for either external illumination using a monochromator or internal illumination for ultimate dark performance. The quantum efficiency measurements were made using the external configuration as shown in Fig. 7.

B. H2RG Operating Conditions

Several *JWST* affiliated groups (*e.g.* Teledyne, University of Hawaii, University of Arizona, STScI) including the DCL have conducted trade studies to find the optimal *JWST* H2RG operating conditions. Based on these, we concluded that for NIRSpec's 5 μm cutoff HgCdTe H2RGs, the optimal temperature is about T = 38.5 K and the scientific performance degrades only slowly for temperatures up to about T < 46 K.

Of all performance parameters, the one that appears to fall off most rapidly with increasing temperature is pixel operability. On avarage, the hot pixel percentage of *JWST*'s 5 μm cutoff HgCdTe H2RGs doubles roughly every 6 K for temperatures near this optimum. Temperature stability is also very important. We therefore actively control the temperature of NIRSpec's H2RGs to δT < 1 mK on the timescale of a test which is a few weeks.

All of the testing that we report here was done using a Gen-III "Leach controller" by Astronomcal Research Cameras Inc. for H2RG control. The Leach controller's video bandwidth is set by a simple RC filter to about 160 kHz. We clock the H2RGs at a pixel rate of 100 kHz per output and use four video outputs. Tab. 3 lists the bias voltages that we used.

The Leach controller's video gain is about 20×. The 16 bit analog to digital converters have a 5 V range resulting in a video gain of about $0.262 \pm .03$ DN μV^{-1} referenced to the video input. With a mean 5 μm cutoff H2RG transimpedance gain of 4.14 μV e^-, this produces a conversion gain of approximately 0.92 e^- DN^{-1}. The measured transimpedance and conversion gains for all parts are shown in Tab. 1.

Table 3: *JWST* NIRSpec Bias Voltages

Bias voltage	Description	Value (V)
Dsub	Detector substrate voltage	0.5
Vreset	Detector reset voltage	0.25
Biaspower	Source node of the internal current source for the pixel source followers	3.28
Biasgate	Bias voltage for the current source of the pixel source followers	2.33
Celldrain	Drain node of the pixel source followers	0
Buffer power	Power for output source follower	3.3
Drain	Drain node of output source follower	0.6
Vdda	Analog power	3.3
Vdd	Digital power	3.3

REFERENCES

Anderson, R. E., Regan, M., Valenti, J., & Bergeron, E. 2014, arXiv, 4181

Bacon, C. M., McMurtry, C. W., Pipher, J. L., Forrest, W. J., & Garnett, J. D. 2005, Focal Plane Arrays for Space Telescopes II. Edited by Grycewicz, 5902, 116

Fano, U. 1947, Physical Review, 72, 26

Leisenring, J., Rieke, M., Misselt, K., & Kiminki, D. 2014, in preparation, 1

McCullough, P. R., Regan, M., Bergeron, L., & Lindsay, K. 2008, Publications of the Astronomical Society of the Pacific, 120, 759

Moore, A. C., Ninkov, Z., & Forrest, W. J. 2004, Focal Plane Arrays for Space Telescopes. Edited by Grycewicz, 5167, 204

Moseley, S. H., Arendt, R. G., Fixsen, D. J., et al. 2010, Proc SPIE, 7742, 36

Mott, D. B., Waczynski, A., Wen, Y., et al. 2007, Proc SPIE, 6690, 18

—. 2008, Proc SPIE, 7021, 66

Podobedov, V. B., Eppeldauer, G. P., & Larason, T. C. 2012, in SPIE Optical Systems Design, ed. L. Mazuray, R. Wartmann, A. P. Wood, M. C. de la Fuente, J.-L. M. Tissot, J. M. Raynor,

T. E. Kidger, S. David, P. Benítez, D. G. Smith, F. Wyrowski, & A. Erdmann (SPIE), 855029

Rauscher, B., Arendt, R. G., Fixsen, D. J., et al. 2013a, Proc SPIE, 1

Rauscher, B. J., Lindler, D. J., Mott, D. B., et al. 2011a, Publications of the Astronomical Society of the Pacific, 123, 953

Rauscher, B. J., Alexander, D., Brambora, C. K., et al. 2007a, Focal Plane Arrays for Space Telescopes III. Edited by Grycewicz, 6690, 19

Rauscher, B. J., Fox, O., Ferruit, P., et al. 2007b, The Publications of the Astronomical Society of the Pacific, 119, 768

Rauscher, B. J., Alexander, D., Brambora, C. K., et al. 2008, High Energy, 7021, 63

Rauscher, B. J., Arendt, R. G., Fixen, D. J., et al. 2011b, Proc SPIE, 8155, 45

Rauscher, B. J., Stahle, C., Hill, R. J., et al. 2012a, AIP Advances, 2, 021901

Rauscher, B. J., Arendt, R. G., Fixsen, D. J., et al. 2012b, Proc SPIE, 8453, 84531F

Rauscher, B. J., Antonille, S. R., Boehm, N., et al. 2013b, Publications of the Astronomical Society of the Pacific, 125, 1465

Shockley, W. 1961, Solid State Electron, 2, 35

Smith, R. M., Zavodny, M., Rahmer, G., & Bonati, M. 2008, in Astronomical Telescopes and Instrumentation: Synergies Between Ground and Space, ed. D. A. Dorn & A. D. Holland (SPIE), 70210J–70210J–12

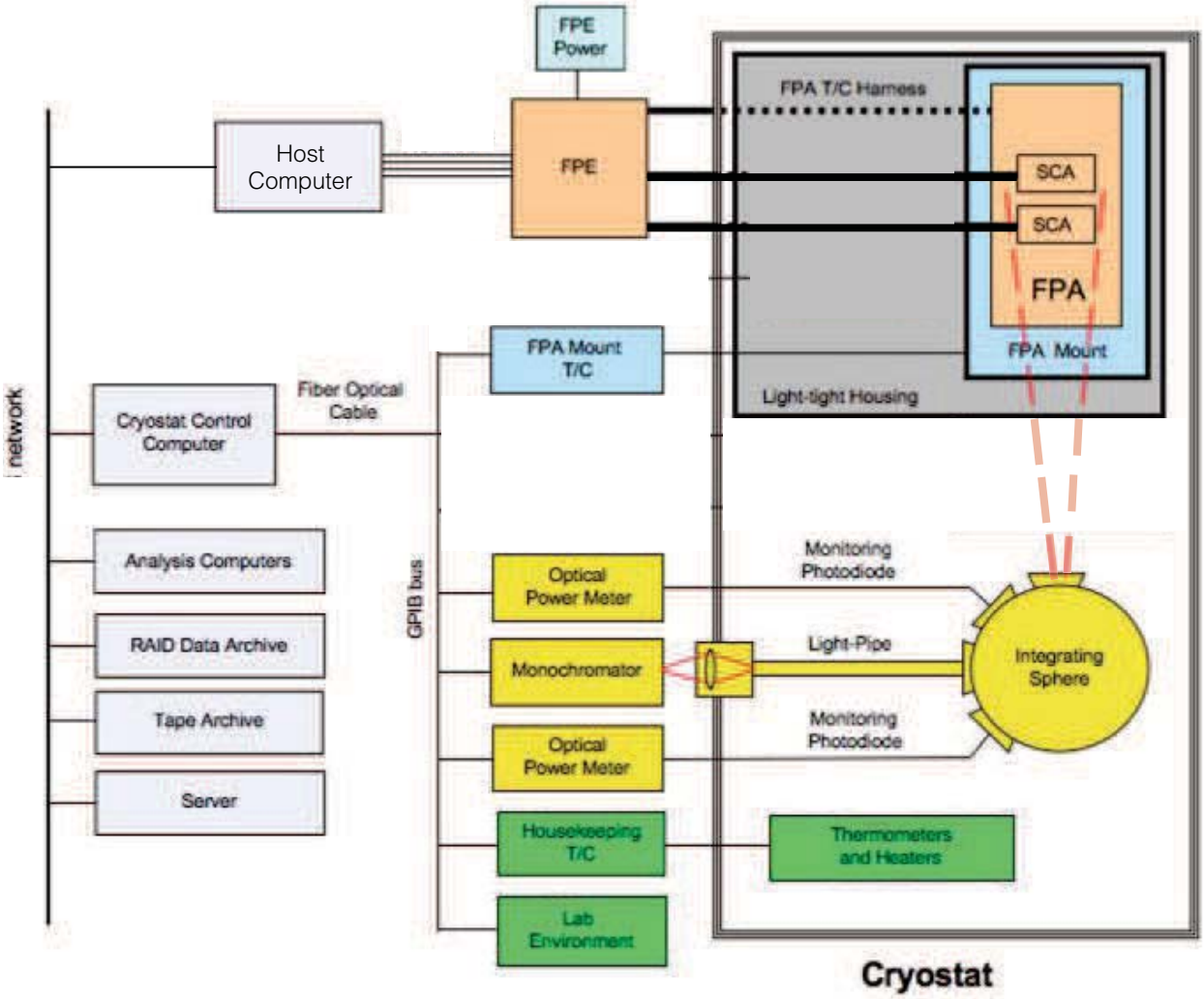

Fig. 7.— The Purple Dewar can be configured for use with either external illumination from a monochromator or internal illumination. For the quantum efficiency measurements that are reported here, we used the external illumination configuration. For these tests, the focal plane electronics (FPE) were a Gen-III Leach controller from Astronomical Research Cameras, Inc, and a Lakeshore temperature controller. Two InSb reference diodes are used to make the measurement. One is permanently mounted in the integrating sphere. This is used to monitor the source intensity prior to all exposures. The second is installed in the focal plane, where it is used to compute the transfer function from the integrating sphere to the focal plane.